Electric-field effects on above-barrier states in a GaAs/$Al_xGa_{1-x}As$ superlattice

Masaaki Nakayama, Masanobu Ando, Isao Tanaka,* and Hitoshi Nishimura
Department of Applied Physics, Faculty of Engineering, Osaka City University, Sugimoto, Sumiyoshi-ku, Osaka 558, Japan

Harald Schneider
Fraunhofer-Institut für Angewandte Festkörperphysik, Tullastrasse 72, D-79108 Freiburg, Germany

Kenzo Fujiwara
Department of Electrical Engineering, Kyushu Institute of Technology, Tobata-ku, Kitakyushu, Fukuoka 804, Japan
(Received 8 August 1994)

We have investigated electric-field effects on the above-barrier states in a GaAs (7.0 nm)/$Al_{0.1}Ga_{0.9}As$ (3.5 nm) superlattice clad by *p*-type and *n*-type $Al_{0.3}Ga_{0.7}As$ layers using electroreflectance spectroscopy for detecting the interband optical transitions and using a transfer-matrix method for calculating the eigenenergies. It is demonstrated that the electric-field dependence of the energies of the optical transitions associated with the above-barrier states exhibits a similar feature of the Stark-ladder states below the barrier potential. In addition, it is found from the line-shape change of the electroreflectance signals that the above-barrier state resonantly couples with the spatially separated below-barrier state. The line-shape change results from the formation of bonding and antibonding states and wave-function delocalization over the coupling space. The transfer-matrix analysis explains the above experimental results reasonably well.

I. INTRODUCTION

In a superlattice (SL) it is well known that long periodicity D causes a mini-Brillouin zone along the growth direction, which results in the formation of the minibands of the electrons and holes. Recently, the effects of an external electric field F on the miniband condition, Wannier-Stark (WS) localization,[1–14] and Franz-Keldysh (FK) oscillation,[15,16] have been considerably investigated in electronic and optical properties. The WS localization, which has especially attracted much attention, results from the breakdown of the resonant tunneling condition by the electrostatic potential difference eFD between neighboring quantum wells (QW's). In the WS localization, the miniband splits into discrete energy states with the equal energy spacing of eFD, the so-called Stark-ladder states; therefore, the energies of the Stark-ladder states are given by $E_0+\nu eFD$, where E_0 is the energy of the miniband center, which corresponds to the eigenenergy in an isolated QW, and ν is the Stark-ladder index, $\nu=0,\pm1,\pm2,\ldots$. If the energy difference between different quantum states ΔE is equal to $meFD$, the Stark-ladder state in a QW resonantly couples with that in the mth nearest-neighbor QW.[7,11,12] The resonant coupling causes the delocalization of the wave function over the coupling space and the formation of the bonding and antibonding states due to wave-function mixing. The above phenomena provide us with the freedom to control the electronic and optical properties of SL's. Until now, the investigation of the electric-field effects has been focused on the energy states below the barrier potential, the so-called below-barrier states. Ritze, Horing, and Enderlein reported the theoretical investigation of the electric-field effects on above-barrier states from the viewpoint of the density of states.[13] They suggested that the above-barrier region is dominated by two kinds of structures: one is similar to FK oscillations, and the other resembles a Stark-ladder behavior. Very recently, Kita *et al.* reported the resonant coupling between the below- and above-barrier states of light holes in an $In_xGa_{1-x}As$/GaAs multiple-QW structure under an applied electric field.[17] Under no electric-field condition, interband optical transitions associated with above-barrier states have been observed by using resonant Raman scattering,[18] photoreflectance,[19] and absorption[20] spectroscopies.

In the present work, we have investigated the electric-field effects on the above-barrier states in an undoped GaAs (7.0 nm)/$Al_{0.1}Ga_{0.9}As$ (3.5 nm) SL clad by *p*-type and *n*-type $Al_{0.3}Ga_{0.7}As$ layers. Electroreflectance (ER) spectroscopy and a transfer-matrix (TM) method with Airy functions have been used to detect the interband optical transitions and to calculate the eigenenergies as a function of electric field, respectively. In our previous works for the WS localization of below-barrier states,[10–12,14] we demonstrated the high sensitivity of ER spectroscopy and the usefulness of the TM method. In the present work, we have clearly detected the optical transitions associated with the above-barrier states in addition to those with the below-barrier states in the electric-field range from ~5 to ~120 kV/cm. The electric-field dependence of the energies of the above-barrier transitions exhibits a similar feature of the Stark-ladder states below the barrier potential. Moreover, we have detected the resonant coupling between the above- and below-barrier states of electrons, heavy holes, and light holes from the changes of the ER line shape and intensity. We discuss the experimental results on the basis of the electric-field dependence of the energies of the

above- and below-barrier states calculated by the TM method.

II. EXPERIMENTAL PROCEDURES

The sample used in the present work was grown on an n-type (001) GaAs substrate by molecular-beam epitaxy (MBE). The SL consists of 70 periods of undoped GaAs (7.0 nm)/$Al_{0.1}Ga_{0.9}As$ (3.5 nm) and is placed in the center of a p-i-n diode structure. The n layer is a Si-doped (1×10^{18} cm^{-3}) $Al_{0.3}Ga_{0.7}As$ (~1 μm thick), and the p layer is a Be-doped (5×10^{18} cm^{-3}) $Al_{0.3}Ga_{0.7}As$ layer (~0.2 μm thick). The sample was processed into a mesa structure with the size of $\sim0.2\times\sim0.9$ mm. The ER measurements were performed at 77 K. The probe light was produced by combination of a 50-W halogen lamp and a 32-cm single monochromator with the resolution of 0.5 nm. The reflected light was detected with a Si photodiode. The applied bias was modulated with the amplitude of 80–200 mV and the frequency of 210 Hz around a given dc bias. We lowered the modulation bias when we measured the fine structures of the ER signals, though the intensity was reduced. The ER signals were obtained by a conventional lock-in technique. In addition, we measured photocurrent (PC) spectra with a picoammeter in order to compare them with the ER spectra.

III. RESULTS AND DISCUSSION

Figure 1 shows the ER spectra of the GaAs (7.0 nm)/$Al_{0.1}Ga_{0.9}As$ (3.5 nm) SL at various electric fields, where the dashed line indicates the band-gap energy of $Al_{0.1}Ga_{0.9}As$. The ER intensities are not normalized with the reflectance intensities because the surface electrode prevents us from obtaining the real reflectance of the SL. The electric field is estimated from the built-in voltage of the p-n junction, 1.45 V, corresponding to the bias voltage on which the Stark-ladder levels below the barrier potential converge. The arrows located on the ER spectrum at 5 kV/cm indicate the energies of the interband transitions calculated by a Kronig-Penney model at zero electric field. In the calculation, the effective-mass parameters including the band nonparabolicities are taken from Ref. 21, and the conduction-band-offset ratio is 0.66. We neglect the exciton-binding energy, which is slightly larger than that (~4 meV) in bulk GaAs because of the miniband formation. The Kronig-Penney-model calculation indicates that the second ($n=2$) electron and light-hole minibands are above the barrier potentials. The notation of Hn_1n_2 (Ln_1n_2) denotes the interband transition associated with the n_1th electron and n_2th heavy-hole (light-hole) minibands, and Γ and π in the parentheses indicate the transition at the Γ and π (mini-Brillouin-zone edge, π/D) points. From the calculated transition energies, it is evident that the ER spectrum at 5 kV/cm reflects the miniband structures below and above the barrier potential. The oscillatory structures in the energy range below 1.6 eV are mainly due to FK oscillations. From Fig. 1, it is obvious that the line shapes and energies of the ER signals remarkably change with increasing the electric field, which will be discussed below. It is noted that we have not clearly observed the above-barrier transitions from the PC spectra.

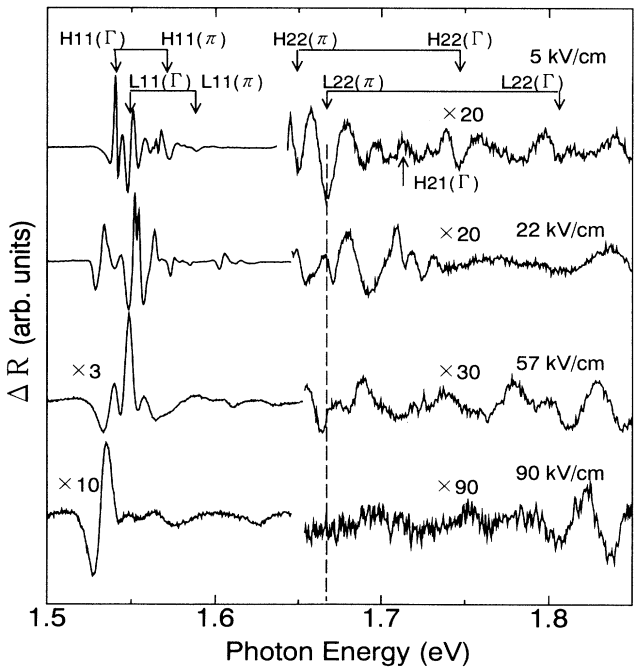

FIG. 1. Electroreflectance spectra of the GaAs (7.0 nm)/$Al_{0.1}Ga_{0.9}As$ (3.5 nm) SL at various electric fields (77 K), where the dashed line indicates the band-gap energy of $Al_{0.1}Ga_{0.9}As$.

The electric-field dependence of the energies of the ER signals is shown in Fig. 2, where the dashed line indicates the band-gap energy of $Al_{0.1}Ga_{0.9}As$, and the vertical arrows on the left side indicate the energy ranges of the miniband transitions at $F=0$ calculated by the Kronig-Penney model. Since the line-shape-analysis method of the ER signals has not yet been revealed, we determine the energies of the $H11(m)$ and $L11(m)$ transitions, comparing the ER spectra with the PC peak profiles, where the number in the parentheses denotes the Stark-ladder index. For other transitions, we adopt the peak energies of the ER signals as the data plotted in Fig. 2; therefore, the energies have uncertainty from ~10 to ~20 meV, which depends on the ER linewidth. It is noted that the electric-field dependence of the dip energies of the ER signals is quite similar to that of the peak energies. From Fig. 2, it is obvious that the electric-field dependence of the energies of the below-barrier transitions labeled $H11(m)$ and $L11(m)$ clearly shows the properties of the Stark-ladder transitions. For the above-barrier transitions labeled $H22$ and $L22$, the electric-field dependence of the energies exhibits the similar feature of that of the Stark-ladder transitions below the barrier potential. The Stark-ladder behaviors of the $H22$ and $L22$ transitions, downward and upward shifts of their energies as a function of electric field, are remarkable in the electric-field range from ~15 to ~30 kV/cm in Fig. 2. The downward shifts above ~30 kV/cm are hidden by the upward ones of the below-barrier transitions. The electric-field dependence of the $H22$- and $L22$-transition energies sug-

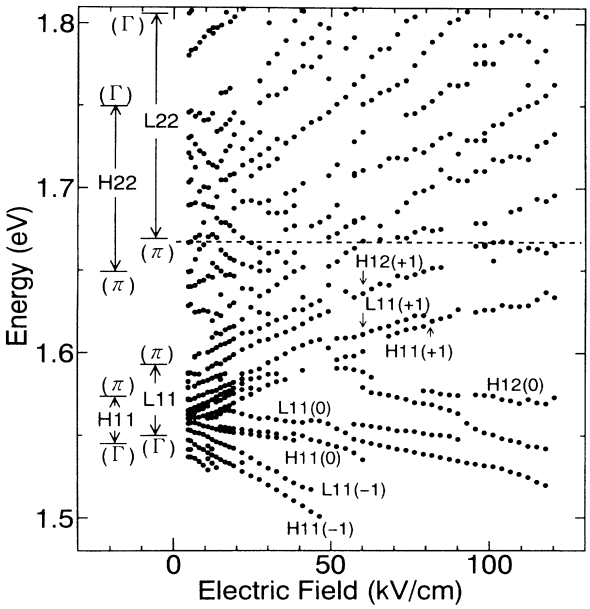

FIG. 2. Electric-field dependence of the ER-signal energies of the GaAs (7.0 nm)/$Al_{0.1}Ga_{0.9}As$ (3.5 nm) SL at 77 K, where the dashed line indicates the band-gap energy of $Al_{0.1}Ga_{0.9}As$, and the vertical arrows on the left side indicate the energy ranges of the miniband transitions at $F=0$ calculated by the Kronig-Penney model.

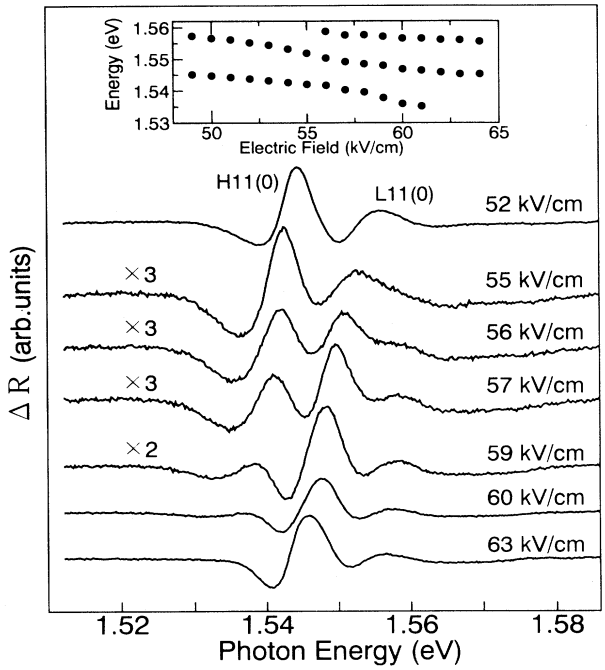

FIG. 3. Electroreflectance spectra of the $H11(0)$ and $L11(0)$ transitions at 77 K around 57 kV/cm, where the inset depicts the electric-field dependence of the ER-signal energies (peak positions), which exhibit the anticrossing.

gests that the Stark-ladder states are formed in the above-barrier region.

Noticing the electric-field dependence of the energies of the $H11(0)$ and $L11(0)$ transitions around 55 and 110 kV/cm in Fig. 2, we clearly find the anticrossing behaviors. According to the previous works[7,11,12] for the resonant coupling between the Stark-ladder states, the anticrossing indicates the occurrence of a resonant coupling between different Stark-ladder states. Figure 3 shows the ER spectra of the $H11(0)$ and $L11(0)$ transitions around 57 kV/cm, and the inset depicts the electric-field dependence of the ER-signal energies (peak positions) that exhibit the anticrossing. Both the $H11(0)$ and $L11(0)$ signals exhibit the splitting feature at 56, 57, 59, and 60 kV/cm, and the intensities are reduced. The ER line shapes at 57 kV/cm are a little different from those in Fig. 1 because of the difference of the modulation bias. The splitting feature is most remarkable at 57 kV/cm, which is the center electric field of the anticrossing behavior shown in the inset of Fig. 3. The splitting and intensity reduction of the ER signals under the resonant-coupling condition result from the formation of the bonding and antibonding states and the decrease of the oscillator strength due to the wave-function delocalization, respectively.[11,12] Since the energy difference between the $H11(0)$ and $L11(0)$ signals is small, ~ 10 meV, the higher-energy part of the doublet $H11(0)$ signals overlaps with the lower-energy part of the doublet $L11(0)$ ones. The simultaneous change of the $H11(0)$ and $L11(0)$ signals indicates that the Stark-ladder state of the $n=1$ electron miniband resonantly couples with another electron state in a spatially separated QW. The Kronig-Penney-model calculation indicates that the energy ranges of the $n \geq 2$ electron minibands are above the barrier potential; therefore, it is expected that the resonant coupling is related to the above-barrier state.

We analyze the above experimental results by using the TM method with Airy functions according to Ref. 22. Our previous works[11,12] have demonstrated that the TM method is quite useful to calculate the Stark-ladder states below the barrier potential in GaAs/AlAs SL's. In the present calculation, the sample structure of the GaAs (7.0 nm)/$Al_{0.1}Ga_{0.9}As$ (3.5 nm) SL is approximated by a system of 11 QW's sandwiched by semi-infinite $Al_{0.3}Ga_{0.7}As$ layers. Transforming the SL growth coordinate z to the dimensionless coordinate Z_j in the Schrödinger equation for an applied electric field F,

$$Z_j=-[2m_j/(e\hbar F)^2]^{1/3}(E-V_j+qFz)\ , \tag{1}$$

we obtain the following TM relation at the interface between the jth and $(j+1)$th layers from the wave-function continuity:

$$\begin{bmatrix} \mathrm{Ai}(Z_j) & \mathrm{Bi}(Z_j) \\ m_j^{-2/3}\mathrm{Ai}'(Z_j) & m_j^{-2/3}\mathrm{Bi}'(Z_j) \end{bmatrix} \begin{bmatrix} a_j \\ b_j \end{bmatrix} = \begin{bmatrix} \mathrm{Ai}(Z_{j+1}) & \mathrm{Bi}(Z_{j+1}) \\ m_{j+1}^{-2/3}\mathrm{Ai}'(Z_{j+1}) & m_{j+1}^{-2/3}\mathrm{Bi}'(Z_{j+1}) \end{bmatrix} \begin{bmatrix} a_{j+1} \\ b_{j+1} \end{bmatrix}\ , \tag{2}$$

where m_j and V_j are the effective mass and potential in the jth layer, respectively, $q=-e(+e)$ for electrons (holes), and Ai and Bi are the Airy functions. Under the boundary condition of the wave-function amplitude in the final layer (semi-infinite $Al_{0.3}Ga_{0.7}As$), $(a_f,b_f)=(1,0)$ for $Z_f\rightarrow\infty$ because of Ai(∞)$\rightarrow$0 and Bi(∞)$\rightarrow\infty$, we assume that the energies of the wave-function-transmittance maxima correspond to the eigenenergies. The effective-mass parameters are the same as those used in the Kronig-Penney model, which is applied to calculate the miniband energies at $F=0$. Ritze, Horing, and Enderlein[13] have used the same TM method to calculate the density of states in an above-barrier region.

Figure 4 shows the electric-field dependence of the energies of the electron states in the modeled GaAs (7.0 nm)/$Al_{0.1}Ga_{0.9}As$ (3.5 nm) SL calculated by using the TM method, where the energies are measured with respect to the center of the modeled SL, and the dashed line indicates the barrier potential of electrons. The notation of $En(m)$ means the nth electron miniband and the mth Stark ladder, which is counted from the center QW. The vertical lines on the left side indicate the energy ranges of the minibands at $F=0$ calculated by the Kronig-Penney model. Although the electric-field dependence exhibits the complicated behavior because of the various resonant-coupling-induced anticrossings, we find

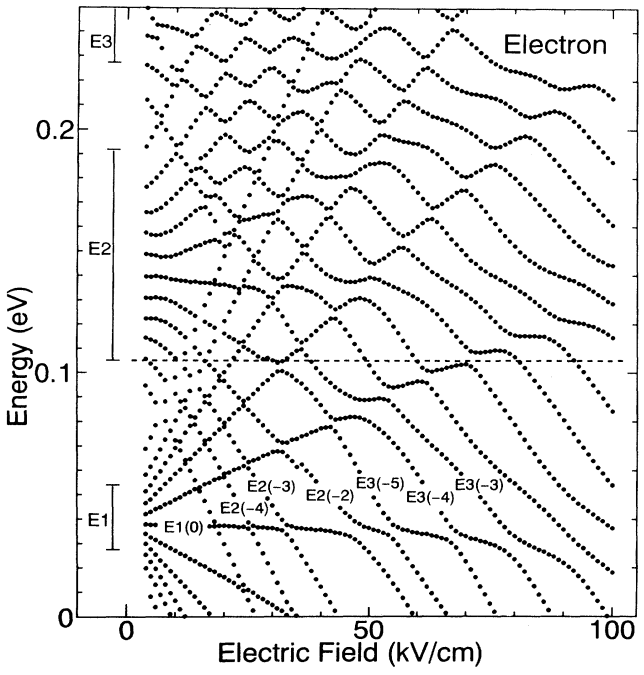

FIG. 4. Electric-field dependence of the energies of the electron states in the modeled GaAs (7.0 nm)/$Al_{0.1}Ga_{0.9}As$ (3.5 nm) SL calculated by using the TM method, where the energies are measured with respect to the center of the modeled SL, and the dashed line indicates the barrier potential of electrons. The notation of $En(m)$ means the nth electron miniband and the mth Stark ladder, which is counted from the center QW. The vertical lines on the left side indicate the energy ranges of the minibands at $F=0$ calculated by the Kronig-Penney model.

that both the below- and above-barrier minibands transform into the Stark-ladder states with increasing electric field. This is consistent with the theoretical results reported by Ritze, Horigin, and Enderlein.[13] As shown in Fig. 2, the electric-field dependence of the observed transition energies associated with the above-barrier states, $H22$ and $L22$, exhibits the similar feature of the Stark-ladder transitions with the below-barrier states, $H11$ and $L11$. Thus, both the experimental and theoretical results demonstrate the formation of the Stark-ladder states of the $E2$ miniband above the barrier potential.

We discuss the anticrossing behaviors of the Stark-ladder states. As described above with Figs. 2 and 3, we clearly observe the anticrossing due to the resonant coupling between the $n=1$ electron state and the above-barrier state, which results in the ER-signal splitting of the $H11(0)$ and $L11(0)$ transitions around 57 kV/cm. In the calculated results of the electron-state energies (Fig. 4), there are two types of the anticrossings between the below-barrier ($E1$) state and the above-barrier ($E2$ and $E3$) states in this electric-field range: For the $E1(0)$ state in the center QW, one around 48 kV/cm is due to the resonant coupling between the $E1(0)$ and $E2(-2)$ states, which is denoted as $E1(0)$-$E2(-2)$, and the other around 55 kV/cm is the $E1(0)$-$E3(-5)$ coupling. On the other hand, we observe only one type of the anticrossing as shown in Fig. 2. From Fig. 4, the TM calculation predicts that the $E3$-related anticrossings of $E1(0)$-$E3(-4)$ and $E1(0)$-$E3(-3)$ occur around 68 and 80 kV/cm, respectively; however, we could not observe them from the ER spectra. Therefore, the observed anticrossing around 57 kV/cm is attributable to the $E1(0)$-$E2(-2)$ coupling. The missing of the $E3$-related coupling in the experiments indicates that the TM calculation of the $E3$ states is quite inaccurate. The energy range of the $E3$ states calculated by the TM method extends over the potential ($\sim$280 meV) of the $Al_{0.3}Ga_{0.7}As$ clad layer. Therefore, we consider the following possible reasons for the inaccuracy of the TM calculation of the $E3$ states. The boundary condition is inappropriate for the $E3$ states, and/or the boundary between the clad layer and the modeled SL remarkably modifies the calculated eigenenergies because of the limited number of the QW's.

From the above discussion, it is concluded that the anticrossing around 57 kV/cm results from the $E1(0)$-$E2(-2)$ coupling, which is the so-called second-nearest-neighbor one. The condition of the mth nearest-neighbor coupling is given by $meFD=\Delta E_{12}$, where ΔE_{12} is the energy difference between the $E1(0)$ and $E2(0)$ states. This indicates that the electric field of the $E1(0)$-$E2(-1)$ coupling is double the value of the $E1(0)$-$E2(-2)$ one; therefore, the anticrossing around 110 kV/cm shown in Fig. 2 is due to the $E1(0)$-$E2(-1)$ coupling. It is noted that the ER signal of the $L11(0)$ transition could not be observed in this high electric field because it is hidden by the broad line width of the strong $H11(0)$ signal owing to a quantum-confined Stark effect. Moreover, the resonant-coupling condition predicts that the third-nearest-neighbor coupling, $E1(0)$-$E2(-3)$, occurs around 38 kV/cm, which is two-thirds of 57 kV/cm for the $E1(0)$-$E2(-2)$ one. Figure 5 shows the ER

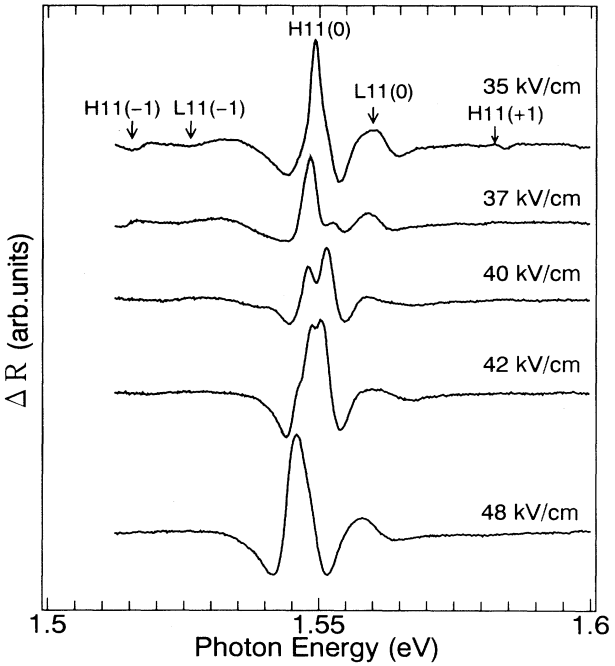

FIG. 5. Electroreflectance spectra of the $H11$ and $L11$ transitions at 77 K around 40 kV/cm, where the third-nearest-neighbor coupling of $E1(0)$-$E2(-3)$ occurs.

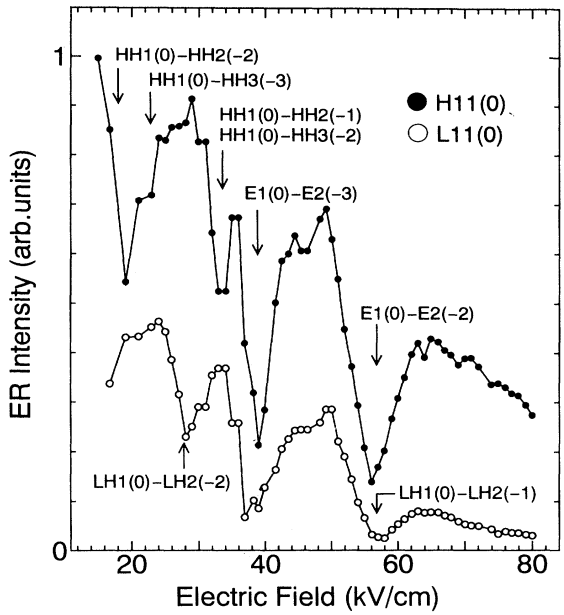

FIG. 6. Electric-field dependence of the ER intensities of the $H11(0)$ and $L11(0)$ transitions at 77 K, where the closed and open circles indicate the $H11(0)$ and $L11(0)$ intensities, and the solid lines are guides to the eye. The several dips result from the various resonant couplings, which are assigned according to the discussion in the text.

spectra of the $H11$ and $L11$ transitions around 40 kV/cm. The $H11(0)$ signal clearly exhibits the splitting feature at 37, 40, and 42 kV/cm. Although we cannot observe the splitting of the $L11(0)$ signal, the intensity is reduced at the above electric fields. In the resonant coupling between the electron states, it is expected that the intensities of both the $H11(0)$ and $L11(0)$ signals decrease because of the delocalization of the electron wave function, which results in the reduction of the oscillator strengths. Thus, we demonstrate the first-, second-, and third-nearest-neighbor couplings between the above-barrier electron state ($E2$) and the below-barrier one ($E1$):$E1(0)$-$E2(-1)$, $E1(0)$-$E2(-2)$, and $E1(0)$-$E2(-3)$. It is noted that the $E2$ states, which produce anticrossings, are WS localized and originate, therefore, not from the miniband edge but from the miniband center, which is significantly above the barrier potential.

Finally, we discuss the ER intensity changes under various resonant coupling conditions. Figure 6 shows the electric-field dependence of the ER intensities of the $H11(0)$ and $L11(0)$ transitions, where the closed and open circles indicate the $H11(0)$ and $L11(0)$ intensities, respectively, and the solid lines are guides to the eye. The typical ER intensity changes around 57 and 40 kV/cm have been already discussed with the ER spectra shown in Figs. 3 and 5, respectively. The ER line shapes change with electric field, so that we adopt the peak-to-dip intensities as the data plotted in Fig. 6. We observe several intensity dips resulting from various resonant couplings. From the above discussion, it is evident that the simultaneous dips of the $H11(0)$ and $L11(0)$ intensities around 57 (40) kV/cm result from the $E1(0)$-$E2(-2)$ [$E1(0)$-$E2(-3)$] coupling. In the resonant coupling between heavy-hole (HH) [light-hole (LH)] states, it is expected that only the $H11(0)$ [$L11(0)$] intensity is reduced by the delocalization of the HH (LH) wave function. Noticing the ER intensities around 19 and 34 (28) kV/cm in Fig. 6, we find that only the $H11(0)$ [$L11(0)$] intensity exhibits the dip profile. This indicates that the resonant coupling between the HH states occurs around 19 and 33 kV/cm and that the LH resonant coupling occurs around 28 kV/cm.

Although we have performed the TM calculation of the hole states, the results are confused and inaccurate because the energies of the hole states are quite close to each other owing to the very low barrier potential of ~ 50 meV. The Kronig-Penney-model calculation at $F=0$ indicates that the center energies of the hole minibands are 11 (HH1), 42 (HH2), 88(HH3), 23 (LH1), and 81 (LH2) meV; therefore, the energy differences between the center energies of the minibands, ΔE_{12}(HH), ΔE_{13}(HH), and ΔE_{12}(LH), are 31, 77, and 58 meV, respectively. The accuracy of the Kronig-Penney calculation is supported by the fact that the calculated transition energies are consistent with the energies of the ER signals at 5 kV/cm as shown in Fig. 1. It is noted that the HH3 and LH2 minibands are the above-barrier ones. From the resonant condition of $meFD=\Delta E_{ij}$ between the ith and jth states, it is expected that the mth-nearest-neighbor coupling between the hole states occurs around the following electric fields: $30/m$ kV/cm for the HH1-HH2 coupling, $73/m$ kV/cm for the HH1-HH3 one, and $55/m$ kV/cm for the LH1-LH2 one. This suggests that the dip of the $H11(0)$ intensity around 34 kV/cm results from the HH1(0)-

HH2(-1) and HH1(0)-HH3(-2) couplings. The narrow dip width of ~ 5 kV/cm indicates that the two types of the resonant couplings simultaneously occur. From the real electric field, 34 kV/cm, of the HH1(0)-HH2(-1) and HH1(0)-HH3(-2) couplings, we consider that the dip of the $H11(0)$ intensity around 18 kV/cm results from the HH1(0)-HH2(-2) and HH1(0)-HH3(-3) couplings, which are expected to occur around 17 (one-half of 34) and 23 (two-thirds of 34) kV/cm, respectively. In this electric-field range from 15 to 30 kV/cm, we observe that only the $H11(0)$ signal continuously exhibits the splitting feature, which appears as the doublet energies of the $H11(0)$ transition as shown in the electric-field dependence of the observed energies (Fig. 2). For the dip of the $L11(0)$ intensity around 28 kV/cm, we consider that it results from the LH1(0)-LH2(-2) coupling because the electric field of the mth nearest-neighbor coupling is given by $55/m$ kV/cm. It seems that the electric field of the LH1(0)-LH2(-1) coupling, which is double the value of the LH1(0)-LH2(-2) one, 56 kV/cm, overlaps with that of the $E1(0)$-$E2(-2)$ one. Thus, it is demonstrated that the Stark-ladder states of the electron, HH, and LH minibands above the barrier potential resonantly couple with the below-barrier states.

IV. CONCLUSIONS

We have investigated the electric-field effects on the above-barrier states in the undoped GaAs (7.0 nm)/$Al_{0.1}Ga_{0.9}As$ (3.5 nm) SL clad by p-type and n-type $Al_{0.3}Ga_{0.7}As$ layers. Electroreflectance spectroscopy and the TM method with Airy functions have been used to detect the interband optical transitions and to calculate the eigenenergies, respectively. It is found that the electric-field dependence of the energies of the above-barrier transitions, $H22$ and $L22$, exhibits a similar feature of the Stark-ladder transitions, $H11$ and $L11$, below the barrier potential. This indicates that the above-barrier minibands transform into the Stark-ladder states with increasing the applied electric field. The Stark-ladder formation of the above-barrier states is explained by the electric-field dependence of the eigenenergies calculated by the TM method. In addition, it is demonstrated that the Stark-ladder states of the $E2$, HH3, and LH2 minibands above the barrier potential resonantly couple with the spatially separated below-barrier states, $E1$, HH1, and LH1, from the line-shape splitting and the intensity reduction of the $H11(0)$ and $L11(0)$ signals, resulting from the formation of the bonding and antibonding states and the wave-function delocalization over the coupling space.

ACKNOWLEDGMENTS

The authors are grateful to K. Kanamoto (Mitsubishi Electric Corporation) for the MBE growth of the sample. This work was supported in part by Grant-in-Aid for Joint Research, Grant No. 05044109, from the Ministry of Education, Science, and Culture in Japan.

*Present address: Science and Technical Research Laboratories of NHK, Kinuta, Setagaya-ku, Tokyo 157, Japan.

[1]J. Bleuse, G. Bastard, and P. Voisin, Phys. Rev. Lett. **60**, 220 (1988).

[2]E. E. Mendez, F. Agulló-Rueda, and J. M. Hong, Phys. Rev. Lett. **60**, 2426 (1988).

[3]P. Voisin, J. Bleuse, C. Bouche, S. Gaillard, C. Alibert, and A. Regreny, Phys. Rev. Lett. **61**, 1639 (1988).

[4]F. Agulló-Rueda, E. E. Mendez, and J. M. Hong, Phys. Rev. B **40**, 1357 (1989).

[5]K. Fujiwara, Jpn. J. Appl. Phys. **28**, L1718 (1989).

[6]B. Soucail, N. Dupuis, R. Ferreira, P. Voisin, A. P. Roth, D. Morris, K. Gibb, and L. Lacelle, Phys. Rev. B **41**, 8568 (1990).

[7]H. Schneider, H. T. Grahn, K. V. Klitzing, and K. Ploog, Phys. Rev. Lett. **65**, 2720 (1990).

[8]R. P. Leavitt and J. W. Little, Phys. Rev. B **42**, 11 784 (1990).

[9]M. M. Dignam and J. E. Sipe, Phys. Rev. B **43**, 4097 (1991).

[10]M. Nakayama, I. Tanaka, T. Doguchi, H. Nishimura, K. Kawashima, and K. Fujiwara, Solid State Commun. **77**, 303 (1991).

[11]M. Nakayama, I. Tanaka, H. Nishimura, K. Kawashima, and K. Fujiwara, Phys. Rev. B **44**, 5935 (1991).

[12]I. Tanaka, M. Nakayama, H. Nishimura, K. Kawashima, and K. Fujiwara, Phys. Rev. B **46**, 7656 (1992).

[13]M. Ritze, N. J. M. Horing, and R. Enderlein, Phys. Rev. B **47**, 10 437 (1993).

[14]I. Tanaka, M. Nakayama, H. Nishimura, K. Kawashima, and K. Fujiwara, Phys. Rev. B **48**, 2787 (1993).

[15]H. Schneider, A. Fischer, and K. Ploog, Phys. Rev. B **45**, 6329 (1992).

[16]K. H. Schmidt, N. Linder, G. H. Döhler, H. T. Grahn, K. Ploog, and H. Schenider, Phys. Rev. Lett. **72**, 2769 (1994).

[17]T. Kita, T. Inazumi, H. Nakayama, and T. Nishino, Phys. Rev. B **50**, 2420 (1994).

[18]J. E. Zucker, A. Pinczuk, D. S. Chemla, A. C. Gossard, and W. Wiegmann, Phys. Rev. B **29**, 7065 (1984).

[19]S. H. Pan, H. Shen, Z. Hang, F. H. Pollak, W. Zhuang, Q. Xu, A. P. Roth, R. A. Masut, C. Lacelle, and D. Morris, Phys. Rev. B **38**, 3375 (1988).

[20]F. C. Zhang, N. Dai, H. Luo, N. Samarth, M. Doborowolska, J. K. Furdyna, and L. R. Ram-Mohan, Phys. Rev. Lett. **68**, 3220 (1992).

[21]D. F. Nelson, R. C. Miller, C. W. Tu, and S. K. Sputz, Phys. Rev. B **36**, 8063 (1987).

[22]D. C. Hutchings, Appl. Phys. Lett. **55**, 1082 (1989).